Sparse Nonlinear System Identification for Hypersonic Aerothermoelastic Analysis with Stochastic Loads

Damien Guého*, Puneet Singla†, Daning Huang‡
Department of Aerospace Engineering, Pennsylvania State University, Univeristy Park, PA-16802

Air-breathing hypersonic vehicles is a class of vehicles that operates at high Mach number in the atmosphere for the entire mission profile and are exposed to an extreme aerothermodynamic environment involving stochastic loads. Due to current limited capability of ground tests and the lack of available flight test data, there is a significant degree of uncertainty associated with the aerothermoelastic modeling of hypersonic vehicles and limited ability to alleviate this uncertainty through experimental testing. This work aims to provide a unified and automatic framework to discover governing equations underlying an unknown dynamical system from data measurements. In an appropriate basis, and based on the assumption that the structure of the dynamical model is governed by only a few important terms, the equations are sparse in nature and the resulting model is parsimonious. Solving a well-posed constrained one-norm optimization problem, we obtain a satisfactory zero-norm approximation solution and determine the most prevalent terms in the dynamic governing equations required to accurately represent the collected data.

I. Introduction

The past decade has witnessed a strong interest in airbreathing hypersonic vehicles for low-cost space exploration as well as rapid response to global military threats [1, 2]. During atmospheric flight, the hypersonic vehicles are exposed to extreme and complex aerothermodynamic environments that involve aerodynamic loading and heating combined with stochastic acoustical loads, viz. aero-thermal-acoustical (ATA) loads. In particular, the large deflections of a control surface can lead to flow separation and subsequently shock wave–boundary-layer interactions (SWBLI), resulting in strong and highly unsteady ATA loads on the vehicle structure [3, 4]. The ATA loads lead to degradation of material properties, accumulation of thermal stress, and fatigue in structure that may eventually impact structural integrity and cause aerothermoelastic instabilities. Therefore, the characterization of the interaction between the ATA loads and the structural response is critical for analyzing performance, stability, and reliability of hypersonic vehicles.

A problem representative of the interaction between the ATA loads and the structure is the panel flutter analysis. Panel flutter is a classical aeroelastic problem and has been studied extensively since late 1950s, as shown in some comprehensive reviews [5, 6]. Furthermore, the inclusion of thermal effects in panel flutter analysis has led to a large body of research in aerothermoelastic analysis [1, 7]. However, while it has been shown that the acoustical loads due to turbulent boundary layer can significantly alter the aerothermoelastic stability boundary of a hypersonic skin panel structure [8], the combined impact of the aerothermal and the acoustical loads on the thermoelastic response has not been studied in depth.

One of the major challenges associated with aerothermoelastic analysis of skin panels involving stochastic loads is the computational cost required for time-resolved analysis. On one hand, due to the high-frequency turbulent flow components, a small time step size on the order of 10^{-3}ms is required to resolve the stochastic structural excitation. On the other hand, high-fidelity finite-element-based structural model is required to capture the nonlinearity that is critical to the aerothermoelastic stability and material response. The combined requirement of the nonlinear modeling and high time resolution leads an intractable computational burden. To tackle this computational challenge, we propose to develop a novel sparse nonlinear system identification technique to generate a reduced-order model (ROM) for the structural model. This new ROM will enable computationally efficient stochastic aerothermoelastic analysis and will pave the way for parametric study and design of robust hypersonic structures in the presence of stochastic aero-thermal-acoustical loads.

*PhD Candidate, Department of Aerospace Engineering, Pennsylvania State University, University Park, PA-16802, Email: djg76@psu.edu.
†Professor, AIAA Associate Fellow, AAS Fellow, Department of Aerospace Engineering, Pennsylvania State University, University Park, PA-16802, Email: psingla@psu.edu.
‡Assistant Professor, AIAA Member, Department of Aerospace Engineering, Pennsylvania State University, University Park, PA-16802, Email: daning@psu.edu.

Historically, system identification for nonlinear dynamical systems has been developed while focusing on specific classes of system and can be broadly categorized into basic approaches such as Volterra series models, block-structured models, NARMAX models, state-space models and neural network models. Rapidly, methods to learn compact representations of signals were developed and have been widely studied in many forms such as factor analysis, and promising performances have been reached in numerous signal processing tasks such as image denoising [9–13], super resolution [14–16], inpainting [17, 18] and compression [19, 20]. Recent advances in machine learning, data science and data modeling have promised the hope of extracting relevant features of dynamical systems and repetitive patterns in vast multimodal data that are beyond the ability of the analyst. However, despite the abundance of experimental data and the development of new technologies, the ability of these algorithms to extrapolate a general physical model and find governing equations from data has been very limited, especially beyond the scope of the domain where they were sampled and constructed. Using symbolic regression, Bongard and Lipson proposed a new approach to determine the underlying structure of a nonlinear dynamical system from data. Techniques that address aspects of the dynamical system discovery problem include the analysis of time-series data [21], methods based on equation-free modeling [22], empirical dynamic modeling [23, 24], modeling emergent behavior [25], and automated inference of dynamics [27–29]. More recently, the dynamical system discovery problem from the perspective of sparse regression and compressed sensing has been addressed by leveraging the fact that most physical systems have only a few relevant terms that define the dynamics, making the governing equations sparse in a high-dimensional nonlinear function space [30]. We aim to build our work upon this last assumption. Sparse regression is employed to determine the most prevalent terms in the dynamic governing equations required to accurately represent the collected data. In the details, we build a dictionary consisting of a complete set of basis functions whose time-series are represented as columns of a matrix. Solving a well-posed constrained ℓ_1 optimization problem provides the most prevalent basis functions that explain the data in the sense of minimizing the $2-$norm of the residuals. After introducing the methodology of sparse representation and how sparse minimization is applied to a general dynamical model, the developed algorithm is applied to a simulated system modeling a heated panel under aerothermoelastic loads.

II. General Methodology

A. Introduction on Sparse Representation

This work aims to present an extended, unified and automatic framework to discover governing equations for aerothermoelastic analysis simply from data measurements, based on the assumption that the structure of the dynamical model is governed by only a few important terms. Considering a general dynamical model with affine control input

$$\dot{\boldsymbol{x}}(t) = \boldsymbol{f}(\boldsymbol{x}(t)) + G\boldsymbol{u}(t), \tag{1}$$

where $\boldsymbol{x}(t) \in \mathbb{R}^n$ represents the state of the system and $\boldsymbol{u}(t) \in \mathbb{R}^r$ the control action at time t and $G \in \mathbb{R}^{n\times r}$ is the constant-time input influence matrix. The unknown nonlinear function $\boldsymbol{f} : \mathbb{R}^n \to \mathbb{R}^n$ represents the dynamics constraints for the system. The goal here is to find to structure of the unknown function $\boldsymbol{f}$ given the time history of $\boldsymbol{x}(t)$ and $\boldsymbol{u}(t)$ and constant control influence matrix, G. Considering a set of basis functions $\{\phi_i\}_{i=1\ldots\infty}, \phi_i : \mathbb{R}^n \to \mathbb{R}$, $\boldsymbol{f}$ can be approximated as a linear combination of these basis function such that $\forall\ \boldsymbol{x} \in \mathbb{R}^n$,

$$\boldsymbol{f}(\boldsymbol{x}) = \sum_{i=1}^{\infty} \boldsymbol{\alpha}_i \phi_i(\boldsymbol{x}), \tag{2}$$

where $\{\boldsymbol{\alpha}_i\}_{i=1..\infty}, \boldsymbol{\alpha}_i \in \mathbb{R}^n$, is a set of unknown coefficients. There are infinitely many choices for basis functions such as polynomials, trigonometric functions, radial basis functions, etc. A central difficulty in learning $\boldsymbol{f}$ lies in choosing appropriate basis functions and the choice of basis functions unfortunately depends on the characteristics of an unknown input-output map. In an appropriate basis, the equations are often sparse in nature and the resulting model is parsimonious, i..e, a very few of $\boldsymbol{\alpha}_i$ are non-zero. It is desired to choose the basis functions which allow to represent $\boldsymbol{f}$ with as few terms in (2) as possible. In this respect, the summation in (2) is taken over finite number of N basis functions:

$$\boldsymbol{f}(\boldsymbol{x}) \approx \sum_{i=1}^{N} \boldsymbol{\alpha}_i \phi_i(\boldsymbol{x}), \tag{3}$$

or equivalently

$$\boldsymbol{f}(\boldsymbol{x}) \approx \boldsymbol{\alpha}^T \boldsymbol{\phi}(\boldsymbol{x}), \tag{4}$$

where $\boldsymbol{\alpha} = \begin{bmatrix} \boldsymbol{\alpha}_1 & \boldsymbol{\alpha}_2 & \cdots & \boldsymbol{\alpha}_N \end{bmatrix}^T \in \mathbb{R}^{N \times n}$ and $\boldsymbol{\phi}(\boldsymbol{x}) = \begin{bmatrix} \phi_1(\boldsymbol{x}) & \phi_2(\boldsymbol{x}) & \cdots & \phi_N(\boldsymbol{x}) \end{bmatrix}^T \in \mathbb{R}^N$. Our objective is to search some handbook of known functions for a set that best represents the given data. Recent advances in compressed sensing and sparse regression [26] can be exploited to learn these few non-zero terms from an over-complete dictionary of basis functions without performing a combinatorially intractable brute-force search. There is no doubt that the choice of basis function significantly effect the approximation accuracy and complexity of the model. For many known physical systems, the nonlinearities can be represented by only a few term with a judicious choice of basis functions. In this respect, many efforts have focused on the adapting the architecture of the network by selecting appropriate models from a pre-defined dictionary of models [27–29]. However, this leads to an exhaustive search algorithm to learn the appropriate basis functions to represent the network dynamics. More recently, advances in compressed sensing and sparse regression has been exploited to learn appropriate basis functions from an over-complete dictionary of basis functions without performing an exhaustive search [30, 31]. To determine the form of the dynamics from data, the authors in these papers collect a time-history of the state and its derivative sampled at a number of instances in time. In the case where the derivative is not part of the measurement model, they construct state derivative information by finite difference methods which make derivative calculations susceptible to noise in measurements. After carefully arranging relevant basis functions in a dictionary, a linear least square problem can be posed to fund unknown coefficients of the basis functions. To enforce sparsity, an iterative least-squares problem is solved where the size of dictionary is reduced by removing basis functions whose amplitude is lower than a prescribed threshold. Though this guarantees the balance between model complexity and accuracy but the resulting algorithm is susceptible to noise in state measurement. As an extension of this work, the main objective of this paper is to consider an integral form of the differential equation to estimate unknown amplitudes of basis functions with only state and input measurements [32]. The secondary objective of this work is to generalize this approach for identification of second and higher order systems with only position level measurement data and system input data. Furthermore, the iterative least squares problem is replaced with an iterative regularized ℓ_1 optimization problem as used in our earlier work on sparse collocation methods for optimal feedback control laws [33]. This guarantees that the sparse solution is found with high probability using convex optimization methods.
The next Section provides the mathematical details corresponding to finding a sparse solution for $\boldsymbol{\alpha}_i's$.

B. Mathematical Development

As stated in the previous Section, the objective is to find a sparse solution for $\boldsymbol{\alpha}_i's$ given the time histories of $\boldsymbol{x}(t)$ and $\boldsymbol{u}(t)$. If time history of $\dot{\boldsymbol{x}}(t)$ is known, then one can solve for the unknown coefficients, $\boldsymbol{\alpha}_i's$ through a least squares solution. In Refs. [30], an iterative least squares problem is solved to find the best set of basis functions to represent $\boldsymbol{f}$ accurately. If time derivative of $\boldsymbol{x}(t)$ is not available, then one needs to reconstruct this information through time history knowledge of $\boldsymbol{x}(t)$ via finite difference. Such an approach is sensitive to noise in measurements of $\boldsymbol{x}(t)$ [30]. In this section, a formulation is presented to find unknown $\boldsymbol{\alpha}_i's$ without any knowledge of $\dot{\boldsymbol{x}}(t)$. First, this formulation is presented for the first-order systems and then generalized for second-order systems.

1. First-order systems

Considering a first-order system, (1) can be rewritten as

$$\dot{\boldsymbol{x}}(t) = \sum_{i=1}^{N} \boldsymbol{\alpha}_i \phi_i(\boldsymbol{x}) + G\boldsymbol{u}(t) \tag{5}$$

and its Laplace transform, component by component along the dimension of $\boldsymbol{x}$, is

$$X_j^{0\mathrm{f}}(s) = sX_j(s) - x_j(0) = \sum_{i=1}^{N} \alpha_{j,i} \Phi_i(s) + \sum_{k=1}^{r} G_{j,k} U_k(s), \;\; j = 1 \ldots n, \tag{6}$$

where $\mathcal{L}\{x_j(t)\} = X_j(s), \mathcal{L}\{\phi_i(\boldsymbol{x})\} = \Phi_i(s), \mathcal{L}\{u_k(t)\} = U_k(s)$ and s is the Laplace variable. Note that $\phi_i(\boldsymbol{x})$ is an implicit function of time and hence, the Laplace transform of this time varying signal can be considered. From now on,

capital letters are used for functions in the Laplace domain. $X_j^{0\mathrm{f}}(s)$ is the original filtered signal (filtered 0-th time). For $\lambda_1 \in \mathbb{R}_+^*$, let us consider the Laplace filtering operator

$$\begin{array}{rccc} \mathcal{I}_{\lambda_1}: & \mathbb{R} & \to & \mathbb{R}, \\ & \bullet & \mapsto & \dfrac{\bullet}{s+\lambda_1}. \end{array} \tag{7}$$

Applying the operator to the signal $X_j^{0\mathrm{f}}$ yields

$$X_j^{1\mathrm{f}}(s) = \mathcal{I}_{\lambda_1}\left(X_j^{0\mathrm{f}}(s)\right) = \frac{sX_j(s) - x_j(0)}{s+\lambda_1} = \sum_{i=1}^{N} \alpha_{i,j}\Phi_i^{1\mathrm{f}}(s) + \sum_{k=1}^{r} G_{j,k}U_k^{1\mathrm{f}}(s). \tag{8}$$

where,

$$\Phi_i^{1\mathrm{f}}(s) = \frac{\Phi_i(s)}{s+\lambda_1} \quad \text{and} \quad U_k^{1\mathrm{f}}(s) = \frac{U_k(s)}{s+\lambda_1}, \tag{9}$$

The exponent [1] can be seen as "filtered once". Note that the aforementioned equation corresponds to the integral form of (1) with $\lambda_1 = 0$. A non-zero λ_1 allows us to take into account any errors in initial conditions. Now, adding and subtracting $\lambda_1 X_j(s)$ to (8) leads to the following expression

$$X_j^{1\mathrm{f}}(s) = \frac{(s+\lambda_1)X_j(s) - \lambda_1 X_j(s) - x_j(0)}{s+\lambda_1} = X_j(s) + \frac{-\lambda_1 X_j(s) - x_j(0)}{s+\lambda_1} = X_j(s) + Y_{j,1}(s), \tag{10}$$

where

$$Y_{j,1}(s) = \frac{-\lambda_1 X_j(s) - x_j(0)}{(s+\lambda_1)}. \tag{11}$$

(11) can be rewritten as

$$sY_{j,1}(s) + x_j(0) = -\lambda_1 Y_{j,1}(s) - \lambda_1 X_j(s) \tag{12}$$

and its inverse Laplace transform yields the following ODE:

$$\begin{cases} \dot{y}_{j,1}(t) = -\lambda_1 y_{j,1}(t) - \lambda_1 x_j(t), \\ y_{j,1}(0) = -x(0). \end{cases} \tag{13}$$

Similarly, the inverse Laplace transforms for $\Phi_i^{1\mathrm{f}}$ and $U_k^{1\mathrm{f}}$ yield the corresponding first order ODEs:

$$\begin{cases} \dot{\phi}_i^{1\mathrm{f}}(t) = -\lambda_1 \phi_i^{1\mathrm{f}}(t) + \phi_i(\boldsymbol{x}), \;\; i = 1, 2, \ldots, N, \\ \phi_i^{1\mathrm{f}}(0) = 0, \end{cases} \tag{14}$$

$$\begin{cases} \dot{u}_k^{1\mathrm{f}}(t) = -\lambda_1 u_k^{1\mathrm{f}}(t) + u_k(t), \;\; k = 1, 2, \ldots, r, \\ u_k^{1\mathrm{f}}(0) = 0. \end{cases} \tag{15}$$

Notice that if $\lambda_1 = 0$, then ϕ_i^{1f} and u_k^{1f} corresponds to time integration of $\phi_i(x(t))$ and $u_k(t)$. For $\lambda_1 > 0$, the aforementioned equations correspond to stable linear system of equations. By appropriately choosing the λ_1, one can control the how quickly the initial condition response of these equations will go to zero. Finally, the final equation in the time domain can be written as:

$$x_j^{1\mathrm{f}}(t) = x_j(t) + y_{j,1}(t) = \sum_{i=1}^{N} \alpha_{j,i}\phi_i^{1\mathrm{f}}(t) + \sum_{k=1}^{r} G_{j,k}u_k^{1\mathrm{f}}(t). \tag{16}$$

Note that the aforementioned equation provides a linear relationship between filtered signals $x_j^{1\mathrm{f}}(t)$, $u_k^{1\mathrm{f}}(t)$ and $\phi_i^{1\mathrm{f}}(t)$. Furthermore, these filtered signals can be constructed directly from the given time histories of system state and control

input by integrating $N + r + 1$ equations given by (13), (14) and (15). Stacking time histories for $x_j^{1\mathrm{f}}(t)$, $\phi_i^{1\mathrm{f}}(t)$ and $u_k^{1\mathrm{f}}(t)$ leads to the following matrix equation

$$\boldsymbol{x}_j^{1\mathrm{f}} = \boldsymbol{\phi}^{1\mathrm{f}^T}\boldsymbol{\alpha}_j + \left(G_j\boldsymbol{u}^{1\mathrm{f}}\right)^T \tag{17}$$

where $\boldsymbol{x}_j^{1\mathrm{f}} \in \mathbb{R}^{l\times 1}$, $\boldsymbol{\phi}^{1\mathrm{f}} \in \mathbb{R}^{N\times l}$, $\boldsymbol{\alpha}_j \in \mathbb{R}^{N\times 1}$, $G_j \in \mathbb{R}^{1\times r}$ and $\boldsymbol{u}^{1\mathrm{f}} \in \mathbb{R}^{r\times l}$ with l being the number of data points. In this equation, $\boldsymbol{\alpha}_j$ is the j^{th} column of the coefficient matrix $\boldsymbol{\alpha}$ introduced in (4) and G_j is the j^{th} row of the coefficient matrix G introduced in (1).

2. Derivation of a Least-Squares Solution

Now, one can find an optimal value of coefficient vector, $\boldsymbol{\alpha}_j$ through the solution of following weighted two-norm minimization:

$$\boldsymbol{\alpha}_j^\star = \min_{\boldsymbol{\alpha}_j} \frac{1}{2}\boldsymbol{e}^T R\boldsymbol{e}, \;\; \boldsymbol{e} = \boldsymbol{x}_j^{1\mathrm{f}} - \boldsymbol{\phi}^{1\mathrm{f}^T}\boldsymbol{\alpha}_j - \left(G_j\boldsymbol{u}^{1\mathrm{f}}\right)^T \tag{18}$$

The weight matrix R can be chosen appropriately depending upon the noise in the measurement data. Depending upon the size of l and N, the aforementioned optimization problem can be over-determined or underdetermined. In both the cases, one can find the solution with an appropriate pseudo inverse of $\boldsymbol{\phi}^{1\mathrm{f}}$, i.e.,

$$\boldsymbol{\alpha}_j^{\star T} = \left(\boldsymbol{x}_j^{1\mathrm{f}^T} - G_j\boldsymbol{u}^{1\mathrm{f}}\right)\boldsymbol{\phi}^{1\mathrm{f}^\dagger} = \tilde{\boldsymbol{x}}^{1\mathrm{f}}\boldsymbol{\phi}^{1\mathrm{f}^\dagger} \tag{19}$$

where $\tilde{\boldsymbol{x}}_j^{1\mathrm{f}} = \boldsymbol{x}_j^{1\mathrm{f}^T} - G_j\boldsymbol{u}^{1\mathrm{f}}$ and † stands for the pseudo-inverse. $\boldsymbol{\phi}^{1\mathrm{f}^\dagger}$ corresponds to the least square solution for over-determined problem, i.e., $\boldsymbol{\phi}^{1\mathrm{f}^\dagger} = \left(\boldsymbol{\phi}^{1\mathrm{f}^T}R\boldsymbol{\phi}^{1\mathrm{f}}\right)^{-1}\boldsymbol{\phi}^{1\mathrm{f}^T}R$ while $\boldsymbol{\phi}^{1\mathrm{f}^\dagger}$ corresponds to the minimum-norm solution for the under-determined case, i.e., $\boldsymbol{\phi}^{1\mathrm{f}^\dagger} = \boldsymbol{\phi}^{1\mathrm{f}^T}R\left(\boldsymbol{\phi}^{1\mathrm{f}}R\boldsymbol{\phi}^{1\mathrm{f}^T}\right)^{-1}$. This procedure is repeated n times (for $j = 1, 2, \ldots, n$) to compute the full coefficient matrix $\boldsymbol{\alpha}$. Note that one can also compute an estimate for control influence matrix , G through this procedure given that it also appears linearly in (17).

3. Derivation of a Sparse Solution

The $\boldsymbol{\alpha}_j^\star$ corresponds to the optimal solution in terms of minimizing the two-norm of state output error response. However, the two-norm solution is not guaranteed to be sparse in nature and is known to pick all the basis functions in our dictionary especially in the case of noise corrupted measurements. To enforce sparsity, ideally ℓ_0 norm of the coefficient vector $\boldsymbol{\alpha}_j$ needs to be minimized subject to constraints of (17). The ℓ_0 norm corresponds to the cardinality of the coefficient vector and its minimization leads to a non-convex problem. However, the ℓ_0 norm minimization problem can be approximated by an iterative ℓ_1-norm minimization problem which is convex in nature with a guaranteed solution [26].

$$\min_{\boldsymbol{\theta}_j^p} ||W^p\boldsymbol{\theta}_j^p||_1 \tag{20}$$

$$\text{s.t.} \left\|\tilde{\boldsymbol{x}}^{1\mathrm{f}} - \boldsymbol{\theta}_j^{p^T}\boldsymbol{\phi}^{1\mathrm{f}}\right\|_2 \leq \varepsilon \left\|\tilde{\boldsymbol{x}}^{1\mathrm{f}} - \boldsymbol{\alpha}_j^{\star T}\boldsymbol{\phi}^{1\mathrm{f}}\right\|_2, \;\; \varepsilon \geq 1 \tag{21}$$

where p is the iteration, $\boldsymbol{\theta}_j^p$ is the optimization variable, $\tilde{\boldsymbol{x}}^{1\mathrm{f}}$ is the pseudo signal, $\boldsymbol{\phi}^{1\mathrm{f}}$ is the dictionary of basis functions and $\boldsymbol{\alpha}_j^{\star T}$ is the optimal two-norm solution derived in the previous section. Notice that two-norm constraint of (21) corresponds to the satisfaction of (17). Rather than using the equality constraint of (17), a two-norm error is bounded by the optimal pseudo-norm solution with ε being the user-defined relaxation on two-norm error. This allows one to tradeoff sparsity with approximation error. Furthermore W^p is a diagonal matrix containing a known weight w_i for the i^{th} optimization variable. Initially, w_i can be chosen based upon any a-priori knowledge about the structure of $\boldsymbol{f}$, the form of the least-squares solution or can simply be chosen to be one. In the subsequent iterations, the value of w_i is adapted according to the following formula to penalize the coefficients that are smaller than a predefined threshold δ:

$$w_i^p = \frac{1}{\left|\theta_{i,j}^{p-1}\right| + \eta}. \tag{22}$$

η is a small number to avoid division by zero. This iterative procedure is repeated unless the computed coefficients converged within a prescribed tolerance. The solution of this iterative ℓ_1 minimization problem provides us a subset of basis functions from an over-complete dictionary which plays a dominant role in underlying unknown dynamics. An optimal pseudo-inverse solution for coefficients is obtained for only these subset of basis functions. Figure **??** illustrates these steps to obtain the sparse solution.

III. Numerical simulations

The sparse identification algorithm is applied to a panel flutter problem. Specifically, two cases are considered: (1) The flutter of a panel with fixed temperature, which shows a level of chaotic response due to the high thermal stress; (2) The response of the panel with prescribed increasing temperature, which resembles the aerothermoelastic behavior of a panel in hypersonic flow.

A. The Panel Flutter Problem

The supposed unknown nondimensionalized expressions equations are

$$\frac{1}{2}\pi^4 q_1(t) - 5\pi^2 R_T q_1(t) + \frac{5}{4}\pi^4 q_1^3(t) - \frac{4}{3}\lambda q_2(t) + 5\pi^4 q_1(t) q_2^2(t) + \frac{1}{2}\sqrt{\frac{\lambda\mu}{M}} q_1'(t) + \frac{1}{2} q_1''(t) = 0, \tag{23a}$$

$$\frac{4}{3}\lambda q_1(t) + 8\pi^4 q_2(t) - 20\pi^2 R_T q_2(t) + 5\pi^4 q_1^2(t) q_2(t) + 20\pi^4 q_2^3(t) + \frac{1}{2}\sqrt{\frac{\lambda\mu}{M}} q_2'(t) + \frac{1}{2} q_2''(t) = 0. \tag{23b}$$

where q_1 and q_2 are structural modal coordinates, λ is the dynamic pressure quantifying the aerodynamic loading, μ is the mass ratio quantifying the aerodynamic damping effect, R_T is the constant temperature increase in the panel quantifying the thermal stress. When $R_T = 0$, there is a critical value λ_{cr}, such that the panel stays stable when $\lambda < \lambda_{cr}$, but enters limit cycle oscillation when $\lambda > \lambda_{cr}$. When $R_T > 0$, the critical value λ_{cr} still exists. However, the panel may become statically buckled or enter chaotic response instead of being stable, when $\lambda < \lambda_{cr}$.
The training dataset for the identification purpose corresponds to response of the system for ten different realizations (initial condition responses), with initial condition $\boldsymbol{q}(0) = \begin{bmatrix} q_1(0) & 0 & 0 & 0 \end{bmatrix}^\intercal$, $q_1(0)$ being a Gaussian random variable of mean zero and covariance $1e-3$. The data is recorded at a frequency of 500Hz.The initial dictionary of basis function consists of all monomials up to order 4 in the $x_1 - x_2 - x_3 - x_4$ space, resulting in 70 basis functions.

The procedure described Figure 1 ensures that a possible suitable sparse solution is found by solving the convex ℓ_1-norm optimization problem described Eq. (20). First of all, Figure 2 shows the error resulting in the propagation for different initial condition using the least-square solution and the sparse solution. The columns on the left is the propagation for a random signal from the training set whereas the columns on the right concerns an arbitrary signal from the testing set. Although the least-square solution performs satisfactory, this results in an over-fitting since we have more basis functions than necessary. On the other hand, the resulting sparse identified model inherently and automatically balances model complexity (because we assume that the dynamics are sparse in nature) with a little bit more accuracy, avoiding over-fitting the model to the data. Figure 3 displays the coefficients found using a least-square solution and the coefficients from the sparse approximation method. Here, the least-square solution is able to give valuable insights about the dominant basis functions and there is no doubt as for which basis functions are prevalent when looking at the results from the sparse approximation. While the least-square solution is a combination of the 70 basis functions and results in an obvious over-fitting, the sparse solution clearly identifies the predominant basis functions that explain the dynamics better. Figure 4 shows the evolution of the sparse solution coefficients during the iterative procedure; a few iterations are enough to completely determine the solution in every direction. Tables 1, 2, 3 and 4 present the values of the sparse coefficients at the very end of the iterative procedure (after final least-square solution). These identified values appear to be very close to the real ones, up to 5 decimal places.

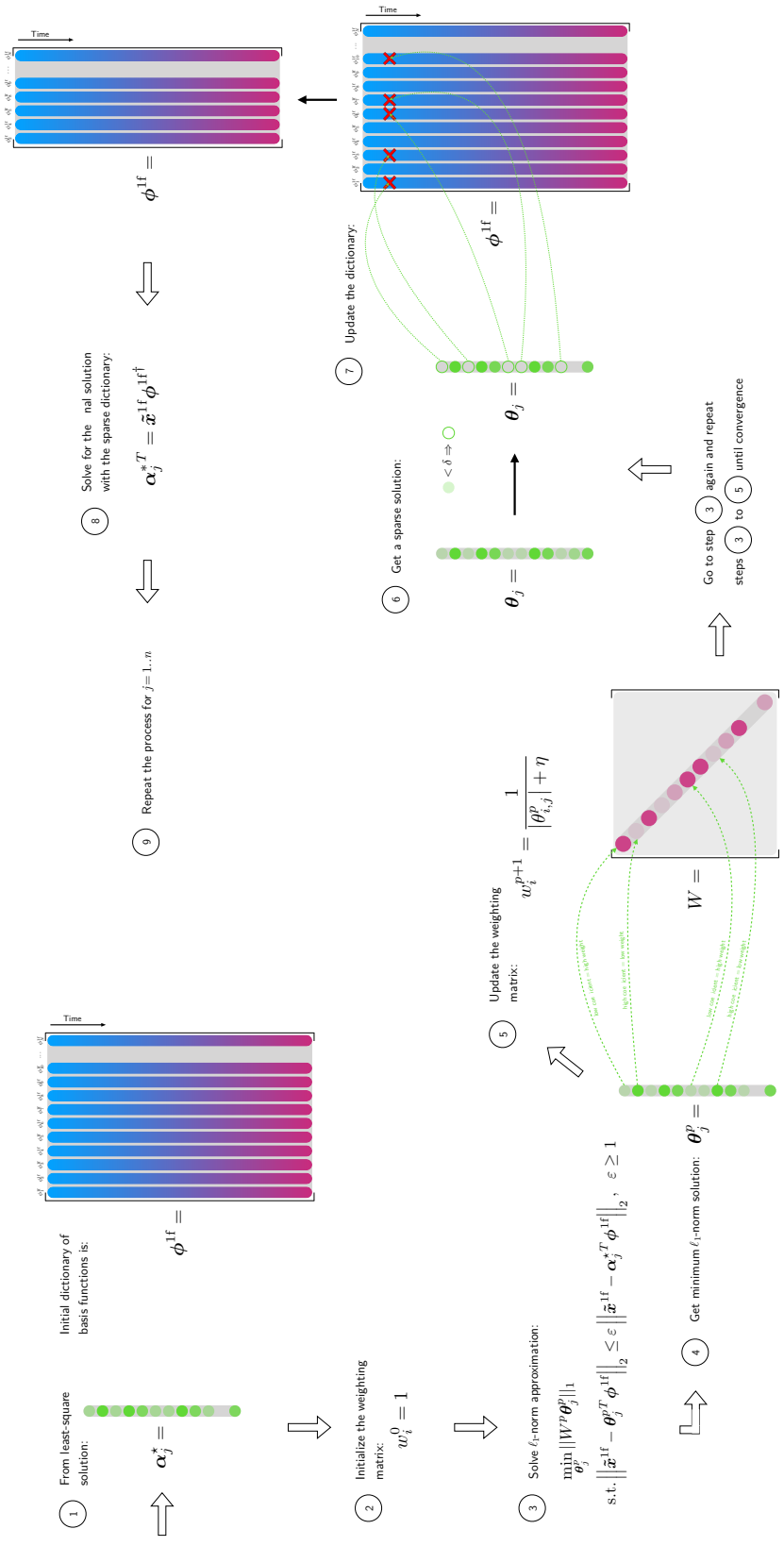

Fig. 1 Illustration of the iterative procedure to derive a sparse solution

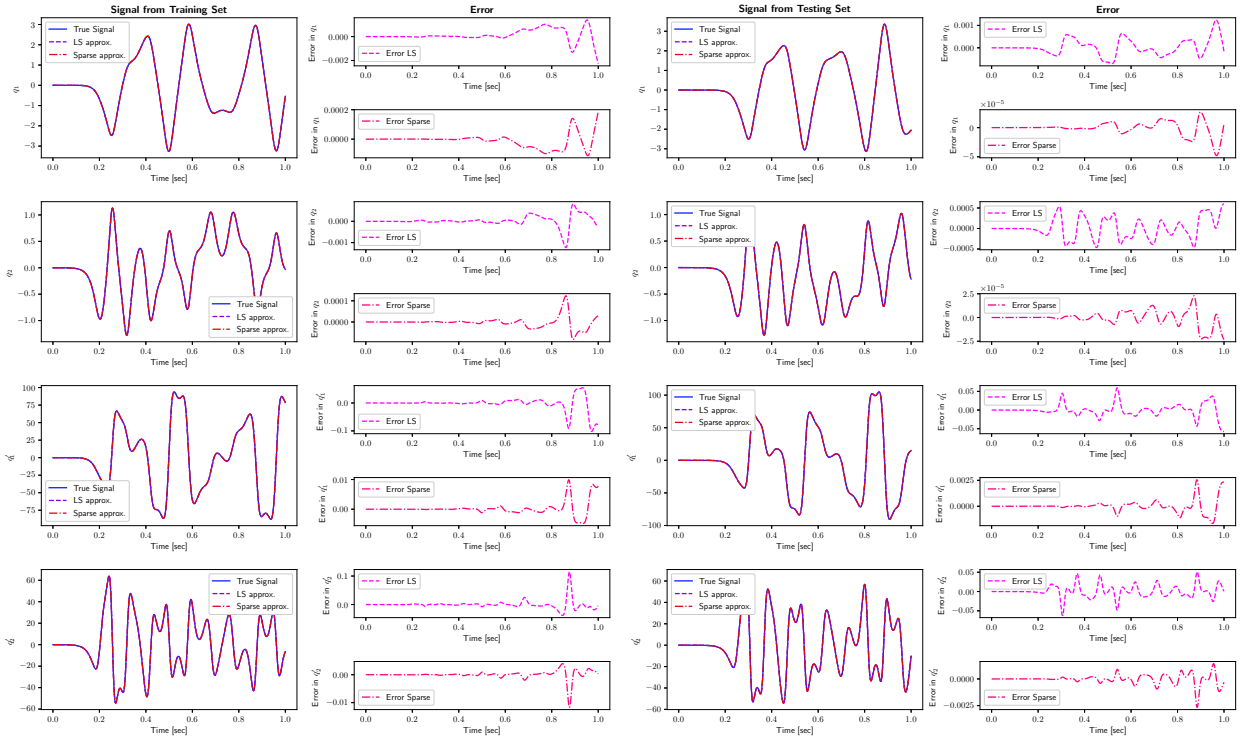

Fig. 2 Error in propagation

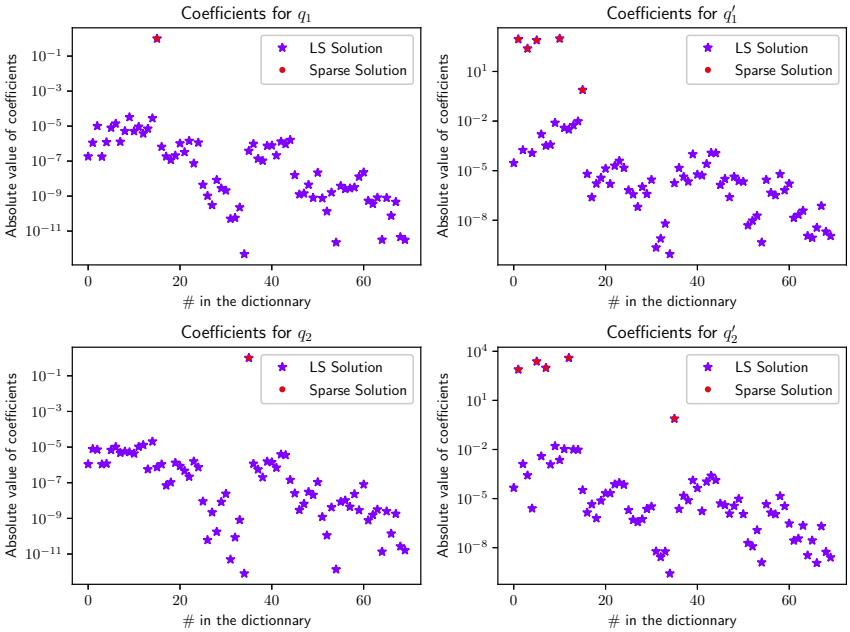

Fig. 3 Coefficients for the least-square solution and the sparse solution (sparse solution is represented on top of the least-square solution)

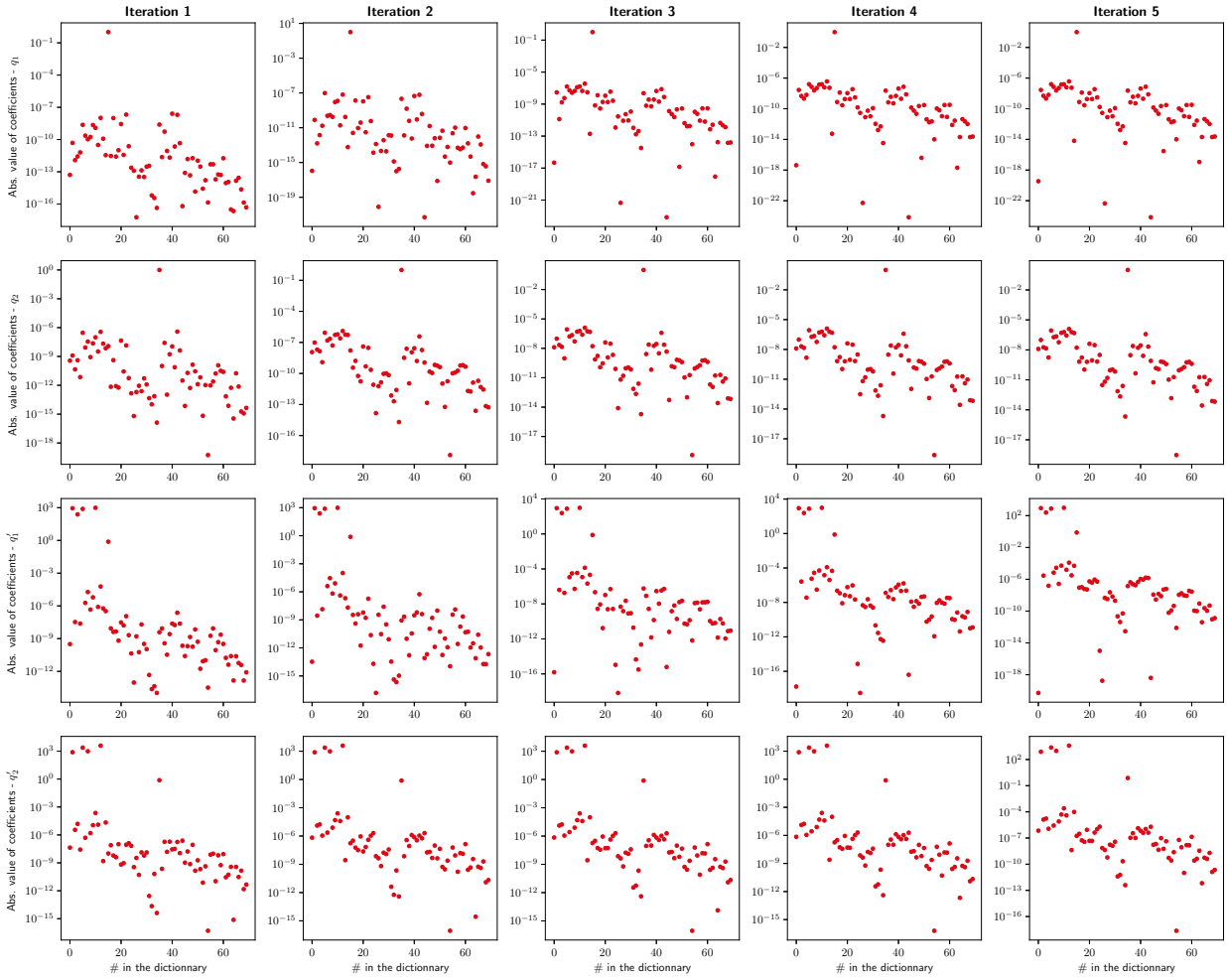

Fig. 4 Iterative values of the sparse coefficients

Table 1 Value of the coefficients for the sparse solution vs the true coefficients - q_1'

Basis Function	# in the dictionary	True Value	Sparse Solution	Relative Error %
$x_1, x_2, x_3, x_4 \mapsto x_3$	15	1	1.00002	$-2 \cdot 10^{-5}$

Table 2 Value of the coefficients for the sparse solution vs the true coefficients - q_2'

Basis Function	# in the dictionary	True Value	Sparse Solution	Relative Error %
$x_1, x_2, x_3, x_4 \mapsto x_4$	35	1	1.00001	$-1 \cdot 10^{-5}$

Table 3 Value of the coefficients for the sparse solution vs the true coefficients - q_1''

Basis Function	# in the dictionary	True Value	Sparse Solution	Relative Error %
$x_1, x_2, x_3, x_4 \mapsto x_1$	1	889.55135	889.55167	$-3.60 \cdot 10^{-5}$
$x_1, x_2, x_3, x_4 \mapsto x_1^3$	3	−243.52273	−243.52277	$-1.64 \cdot 10^{-5}$
$x_1, x_2, x_3, x_4 \mapsto x_2$	5	773.33333	773.33266	$8.66 \cdot 10^{-5}$
$x_1, x_2, x_3, x_4 \mapsto x_1 x_2^2$	10	−974.09091	−974.09220	$-1.32 \cdot 10^{-4}$
$x_1, x_2, x_3, x_4 \mapsto x_3$	15	−0.76157	−0.76123	$4.46 \cdot 10^{-4}$

Table 4 Value of the coefficients for the sparse solution vs the true coefficients - q_2''

Basis Function	# in the dictionary	True Value	Sparse Solution	Relative Error %
$x_1, x_2, x_3, x_4 \mapsto x_1$	1	−773.33333	−773.33436	$-1.33 \cdot 10^{-4}$
$x_1, x_2, x_3, x_4 \mapsto x_2$	7	2389.29630	2389.30681	$-4.40 \cdot 10^{-4}$
$x_1, x_2, x_3, x_4 \mapsto x_1^2 x_2$	9	−974.09091	−974.09264	$-1.78 \cdot 10^{-4}$
$x_1, x_2, x_3, x_4 \mapsto x_2^3$	18	−3896.36364	−3896.37920	$-3.99 \cdot 10^{-4}$
$x_1, x_2, x_3, x_4 \mapsto x_4$	35	−0.76157	−0.76247	$-1.18 \cdot 10^{-3}$

B. The Panel Flutter Problem with time-varying temperature increase

The supposed unknown nondimensionalized expressions equations are a modified set of panel flutter equations

$$\frac{1}{2}\pi^4 q_1(t) - 5\pi^2 R_T q_1(t) + cR_T + \frac{5}{4}\pi^4 q_1^3(t) - \frac{4}{3}\lambda q_2(t) + 5\pi^4 q_1(t) q_2^2(t) + \frac{1}{2}\sqrt{\frac{\lambda\mu}{M}} q_1'(t) + \frac{1}{2} q_1''(t) = 0, \tag{24a}$$

$$\frac{4}{3}\lambda q_1(t) + 8\pi^4 q_2(t) - 20\pi^2 R_T q_2(t) + 5\pi^4 q_1^2(t) q_2(t) + 20\pi^4 q_2^3(t) + \frac{1}{2}\sqrt{\frac{\lambda\mu}{M}} q_2'(t) + \frac{1}{2} q_2''(t) = 0. \tag{24b}$$

$$\dot{R}_T = d \tag{24c}$$

where Eq. (24c) is introduced to characterize the temperature increase in the panel during aerothermoelastic response, and the linear term cR_T in Eq. (24a) is introduced to characterize the effect of nonuniform temperature increase in the thickness direction of a panel.

The training dataset for the identification purpose corresponds to response of the system for ten different realizations (initial condition responses), with initial condition $\boldsymbol{q}(0) = \begin{bmatrix} q_1(0) & 0 & 0 & 0 \end{bmatrix}^\intercal$, $q_1(0)$ being a Gaussian random variable of mean zero and covariance $1e-3$. The data is recorded at a frequency of 1000Hz.The initial dictionary of basis function consists of all monomials up to order 4 in the $x_1 - x_2 - x_3 - x_4 - x_5$ space, resulting in 240 basis functions.

Once again, the procedure presented before is used to find the unknown coefficient vector. Figures 6 displays the least squares as well as the sparse solution for coefficients for both the test cases. While the sparse solution correctly identifies the correct basis functions, the least-squares fit non-zero amplitude for most of the basis functions. Figure 5 shows the resulting error in the propagation for two signals, one belonging to the training set. Tables 5, 6, 7, 8 and 9 present the values of the identified coefficients. These identified values appear to be very close to the true ones which shows the efficacy of the developed methodology in identifying the true dynamics of the system. From these results, it is clear that the proposed sparse approximation solution leads to several orders of magnitude improvement in state propagation errors. This better performance of the sparse approximation method can be attributed to its ability to identify the inherent true dynamics of the system.

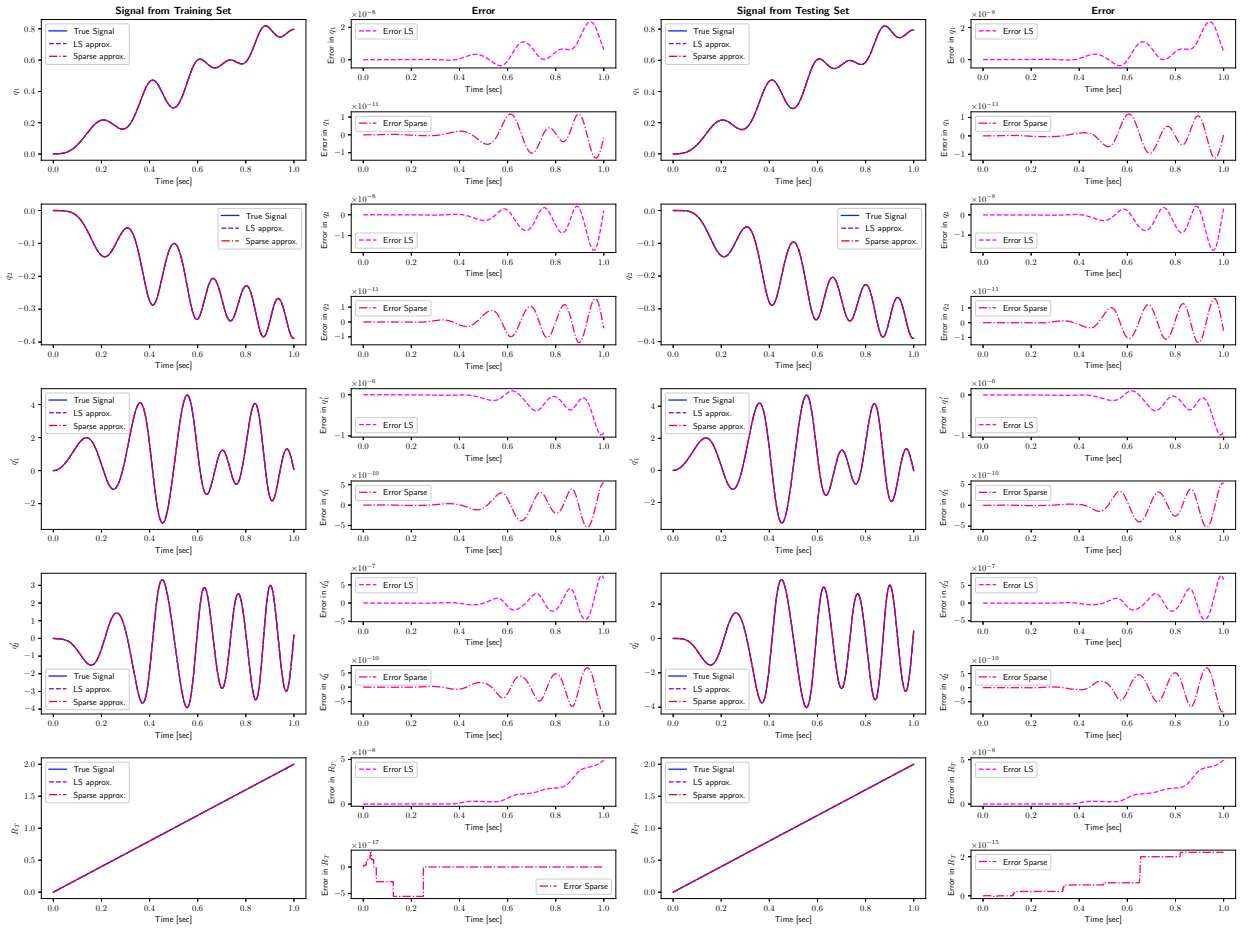

Fig. 5 Error in propagation

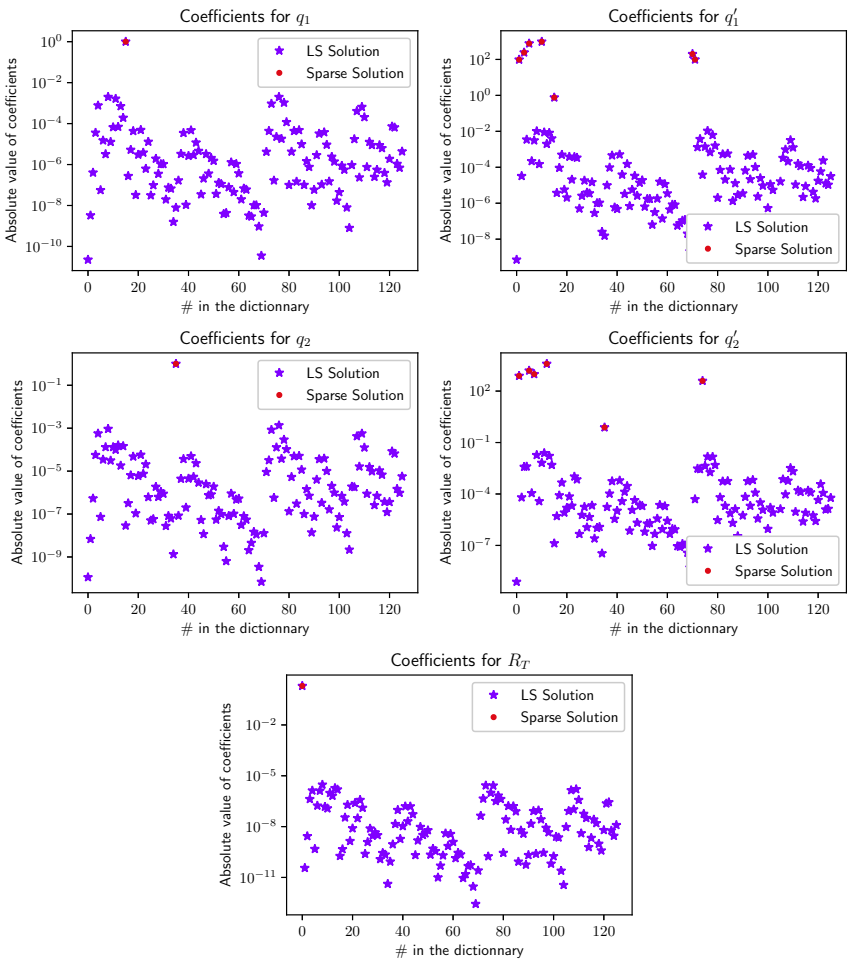

Fig. 6 Coefficients for the least-square solution and the sparse solution (sparse solution is represented on top of the least-square solution)

Table 5 Value of the coefficients for the sparse solution vs the true coefficients - q_1'

Basis Function	# in the dictionary	True Value	Sparse Solution	Relative Error %
$x_1, x_2, x_3, x_4, x_5 \mapsto x_3$	15	1	1.0000	$-1 \cdot 10^{-5}$

Table 6 Value of the coefficients for the sparse solution vs the true coefficients - q_2'

Basis Function	# in the dictionary	True Value	Sparse Solution	Relative Error %
$x_1, x_2, x_3, x_4, x_5 \mapsto x_4$	35	1	1.00001	$-1 \cdot 10^{-5}$

Table 7 Value of the coefficients for the sparse solution vs the true coefficients - q_1''

Basis Function	# in the dictionary	True Value	Sparse Solution	Relative Error %
$x_1, x_2, x_3, x_4, x_5 \mapsto x_1$	1	−97.40909	−97.40956	$-4.83 \cdot 10^{-6}$
$x_1, x_2, x_3, x_4, x_5 \mapsto x_1^3$	3	−243.52273	−243.52271	$8.21 \cdot 10^{-8}$
$x_1, x_2, x_3, x_4, x_5 \mapsto x_2$	5	773.33333	773.33310	$2.97 \cdot 10^{-7}$
$x_1, x_2, x_3, x_4, x_5 \mapsto x_1 x_2^2$	10	−974.09091	−974.09073	$1.85 \cdot 10^{-7}$
$x_1, x_2, x_3, x_4, x_5 \mapsto x_3$	15	−0.76157	−0.76169	$1.58 \cdot 10^{-4}$
$x_1, x_2, x_3, x_4, x_5 \mapsto x_4$	70	200	199.99946	$2.70 \cdot 10^{-6}$
$x_1, x_2, x_3, x_4, x_5 \mapsto x_1 x_4$	71	98.69604	98.69841	$-2.40 \cdot 10^{-5}$

Table 8 Value of the coefficients for the sparse solution vs the true coefficients - q_2''

Basis Function	# in the dictionary	True Value	Sparse Solution	Relative Error %
$x_1, x_2, x_3, x_4, x_5 \mapsto x_1$	1	−773.33333	−773.33192	$1.82 \cdot 10^{-6}$
$x_1, x_2, x_3, x_4, x_5 \mapsto x_2$	5	−1558.54545	−1558.54178	$2.35 \cdot 10^{-6}$
$x_1, x_2, x_3, x_4, x_5 \mapsto x_1^2 x_2$	7	−974.09091	−974.09755	$-6.82 \cdot 10^{-6}$
$x_1, x_2, x_3, x_4, x_5 \mapsto x_2^3$	12	−3896.36364	−3896.36310	$1.39 \cdot 10^{-7}$
$x_1, x_2, x_3, x_4, x_5 \mapsto x_4$	35	−0.76157	−0.76190	$-4.33 \cdot 10^{-4}$
$x_1, x_2, x_3, x_4, x_5 \mapsto x_4$	74	98.69604	98.69617	$-1.32 \cdot 10^{-6}$

Table 9 Value of the coefficients for the sparse solution vs the true coefficients - R_T

Basis Function	# in the dictionary	True Value	Sparse Solution	Relative Error %
$x_1, x_2, x_3, x_4 \mapsto 1$	0	10	10.00001	$-1.00 \cdot 10^{-6}$

IV. Conclusion

This work presents a novel sparse system identification algorithm, a reliable and automatic technique to identify governing equations of nonlinear dynamical systems from measured data. Using Laplace transformations and filtering, the use of an iterative sparse regression algorithm on collected data to find the prevalent basis functions is shown to be successful in explaining the overall dynamics of the systems considered. In the demonstration examples, the algorithm successfully identifies the nonlinear governing equations of (1) a panel flutter system with fixed temperature, and (2) a panel flutter system with time-varying temperature, resembling aerothermoelastic response. In both cases the system parameters are identified with high accuracy, with errors close to zero.

Eventually the algorithm can be applied to build a compact reduced order model for a coupled thermal and structural response in a high-fidelity aerothermoelastic simulation, or wind tunnel measurements for fluid-thermal-structural interactions. High order nonlinear basis functions should be able to specifically capture critical instability behaviors, e.g. thermal buckling and LCO, as well as the nonlinear effects introduced by aerothermal loads with higher-fidelity. The identified nonlinear basis functions are expected to provide valuable insight into the aerothermoelastic behavior during the wind tunnel experiments or from the computational analysis.

V. Acknowledgment

This material is based upon work supported jointly by the AFOSR grants FA9550-17-1- 0088 and FA9550-20-1-0176.

References

[1] J. J. McNamara and P. P. Friedmann. Aeroelastic and Aerothermoelastic Analysis in Hypersonic Flow: Past, Present, and Future. AIAA Journal, 49(6):1089–1122, 2011.

[2] K. G. Bowcutt. Physics drivers of hypersonic vehicle design. In AIAA 2018–5373, 22nd AIAA International Space Planes and Hypersonics Systems and Technologies Conference, pages 1–22, Orlando, FL, Sept 2018.

[3] Dolling, D. S., "Fifty years of shock-wave/boundary-layer interaction research: What next?" AIAA Journal, Vol. 39, No. 8, 2001, pp. 1517–1531.

[4] Babinsky, H., and Harvey, J. K., Shock Wave-Boundary-Layer Interactions, 1st ed., Cambridge University Press, 2012.

[5] Dowell, E. H., Aeroelasticity ofPlates and Shells, Vol. 1, Springer Science & Business Media, 1974.

[6] Mei, C., Abdel-Motagaly, K., and Chen, R., "Review of Nonlinear Panel Flutter at Supersonic and Hypersonic Speeds," Applied Mechanics Reviews, Vol. 52, No. 10,1999, pp. 321–332.

[7] D. Huang. Development of a Hypersonic Aerothermoelastic Framework and Its Application to Flutter and Aerothermoelastic Scaling of Skin Panels. PhD thesis, University of Michigan, Ann Arbor, 2019

[8] Deshmukh, R., Culler, A. J., Miller, B. A., and McNamara, J. J., "Response of Skin Panels to Combined Self-And Boundary Layer-Induced Fluctuating Pressure," Journal ofFluids and Structures, Vol. 58, 2015, pp. 216–235.

[9] Cai, J.F.; Ji, H.; Shen, Z.; Ye, G.B. "Data-driven tight frame construction and image denoising". Appl. Comput. Harmon. Anal. 2014, 37, 89-105.

[10] Xie, J.; Feris, R.S.; Yu, S.S.; Sun, M.T. "Joint super resolution and denoising from a single depth image". IEEE Trans. Multimed. 2015, 17, 1525-1537.

[11] Rubinstein, R.; Zibulevsky, M.; Elad, M. "Efficient Implementation of the KSVD Algorithm and the Batch-OMP Method". Tech. Rep.; Department of Computer Science, Technion: Haifa, Israel, 2008.

[12] Fadili, M.J.; Starck, J.-L.; Murtagh, F. "Inpainting and zooming using sparse representations". Comput. J. 2009, 52, 64-79.

[13] Liu, Y.; Zhai, G.; Gu, K.; Liu, X.; Zhao, D.; Gao, G. "Reduced-reference image quality assessment in free-energy principle and sparse representation". IEEE Trans. Multimed. 2018, 20, 379-391.

[14] Zhao, J.; Hu, H.; Cao, F. "Image super-resolution via adaptive sparse representation". Knowl. Based Syst. 2017, 124, 23-33.

[15] Zhu, Z.; Guo, F.; Yu, H.; Chen, C. "Fast single image super-resolution via self-example learning and sparse representation". IEEE Trans. Multimed. 2014, 16, 2178-2190.

[16] Beck, A.; Teboulle, M. "A fast iterative shrinkage thresholding algorithm for linear inverse problems". SIAM J. Imag. Sci. 2009, 2, 183-202.

[17] Elad, M. "Sparse and Redundant Representations. In From Theory to Applications in Signal and Image Processing"; Springer: Berlin, Germany, 2010.

[18] Zhang, L.; Bioucas-Dias, J.M. "Fast hyperspectral image denoising and inpainting based on low-rank and sparse representations". IEEE J. Sel. Top. Appl. Earth Obs. Remote. Sens. 2018, 11, 730-742.

[19] Kalluri, M.; Jiang, M.; Ling, N.; Zheng, J.; Zhang, P. "Adaptive RD optimal sparse coding with quantization for image compression". IEEE Trans. Multimed. 2019, 21, 39-50.

[20] Liu, Y.; Dimitris A. Pados, "Compressed-sensed-domain l1-pca video surveillance". IEEE Trans. Multimed. 2016, 18, 351-363.

[21] Crutchfield JP, McNamara BS (1987) "Equations of motion from a data series". Complex Syst 1(3):417-452.

[22] Ioannis G. Kevrekidis, C. William Gear, James M. Hyman, Panagiotis G. Kevrekidis, Olof Runborg, and Constantinos Theodoropoulos (2003) "Equation-free, coarse-grained multiscale computation: Enabling microscopic simulators to perform system-level analysis". Commun Math Sci 1(4):715-762.

[23] George Sugihara, Robert May, Hao Ye, Chih-hao Hsieh, Ethan Deyle, Michael Fogarty, Stephan Munch (2012) "Detecting causality in complex ecosystems". Science 338(6106): 496-500.

[24] Ye H, et al. (2015) “Equation-free mechanistic ecosystem forecasting using empirical dynamic modeling". Proc Natl Acad Sci USA 112(13):E1569-E1576.

[25] Roberts AJ (2014) “Model Emergent Dynamics in Complex Systems" (SIAM, Philadelphia).

[26] Boyd, S. and L. Vandenberghe (2004, 67-78, 152-159) Convex Optimization, Cambridge University Press.

[27] Schmidt MD, Vallabhajosyula RR, Jenkins JW, Hood JE, Soni AS, Wikswo JP, Lipson H (2011) “Automated refinement and inference of analytical models for metabolic networks". Phys Biol 8(5):055011.

[28] Daniels BC, Nemenman I (2015) “Automated adaptive inference of phenomenological dynamical models". Nat Commun 6:8133.

[29] Daniels BC, Nemenman I (2015) “Efficient inference of parsimonious phenomenological models of cellular dynamics using S-systems and alternating regression". PLoS One 10(3):e0119821.

[30] Steven L. Bruntona, Joshua L. Proctorb, and J. Nathan Kutzc, “Discovering governing equations from data by sparse identification of nonlinear dynamical systems," Proc Natl Acad Sci USA April 12, 2016 113 (15) 3932-3937; https://doi.org/10.1073/pnas.1517384113

[31] Proctor, J. L., S. L. Brunton, B. W. Brunton, and J. Kutz (2014) “Exploiting sparsity and equation-free architectures in complex systems,” The European Physical Journal Special Topics, 223(13), pp. 2665-2684.

[32] Gueho, D., P. Singla, and R. G. Melton (2020) “Data-Driven Sparse Approximation For The Identification Of Nonlinear Dynamical Systems: Application In Astrodynamics,” in 2020 AAS/AIAA Astrodynamics Specialist Conference.

[33] Adurthi, N., P. Singla, and M. Majji (2017) “Sparse approximation–based collocation scheme for nonlinear optimal feedback control design,” Journal of Guidance, Control, and Dynamics, 40(2), pp. 248-264.